International Journal of Remote Sensing

ISSN: 0143-1161 (Print) 1366-5901 (Online) Journal homepage: https://www.tandfonline.com/loi/tres20

Classification of shoreline vegetation in the Western Basin of Lake Erie using airborne hyperspectral imager HSI2, Pleiades and UAV data

Prabha Amali Rupasinghe, Anita Simic Milas, Kristin Arend, Martin Albert Simonson, Christine Mayer & Scudder Mackey

To cite this article: Prabha Amali Rupasinghe, Anita Simic Milas, Kristin Arend, Martin Albert Simonson, Christine Mayer & Scudder Mackey (2019) Classification of shoreline vegetation in the Western Basin of Lake Erie using airborne hyperspectral imager HSI2, Pleiades and UAV data, International Journal of Remote Sensing, 40:8, 3008-3028, DOI: 10.1080/01431161.2018.1539267

To link to this article: https://doi.org/10.1080/01431161.2018.1539267

Published online: 13 Nov 2018.

INTERNATIONAL JOURNAL OF REMOTE SENSING
2019, VOL. 40, NO. 8, 3008–3028
https://doi.org/10.1080/01431161.2018.1539267

Taylor & Francis
Taylor & Francis Group

Classification of shoreline vegetation in the Western Basin of Lake Erie using airborne hyperspectral imager HSI2, Pleiades and UAV data

Prabha Amali Rupasinghe[a], Anita Simic Milas[a], Kristin Arend[b], Martin Albert Simonson[c], Christine Mayer[c] and Scudder Mackey[d]

[a]Department of Geology, Bowling Green State University, Bowling Green, OH, USA; [b]Ohio Department of Natural Resources, Division of Wildlife, Old Woman Creek National Estuarine Research Reserve, Huron, OH, USA; [c]Department of Environmental Sciences and Lake Erie Centre, University of Toledo, Toledo, OH, USA; [d]Ohio Department of Natural Resources, Office of Coastal Management, Sandusky, OH, USA

ABSTRACT

Mapping land and aquatic vegetation of coastal areas using remote sensing for better management and conservation has been a long-standing interest in many parts of the world. Due to natural complexity and heterogeneity of vegetation cover, various remote sensing sensors and techniques are utilized for monitoring coastal ecosystems. In this study, two unsupervised and two supervised standard pixel-based classifiers were tested to evaluate the mapping performance of the second-generation airborne NASA Glenn Hyperspectral Imager (HSI2) over the narrow coastal area along the Western Lake Erie's shoreline. Furthermore, the classification results of HSI2 (using the whole Visible-Near Infrared (VIS+ NIR) hyperspectral dataset, and also the spectral subset of Visible (VIS) spectral bands) were compared to multispectral Pleiades (VIS+ NIR) and Unmanned Aerial Vehicle (UAV) VIS classified images. The goal was to explore how different spectral ranges, and spatial and spectral resolutions impact the unsupervised and supervised classifiers. While the unsupervised classifiers depended more on the spectral range, spectral or spatial resolutions were important for the supervised classifiers. The Support Vector Machine (SVM) was found to perform better than other classification methods for the HSI2 images over all twenty-two study sites with the overall accuracy (OA) ranging from 82.6%–97.5% for VIS, and 81.5%–95.6 % for VIS + NIR. Considerably better performance of the supervised classifiers for the HSI2 VIS data over the Pleiades data (OA = 74.8–83.4%) suggested the importance of spectral resolution over spectral range (VIS vs. VIS+ NIR) for the supervised methods. The unsupervised classifiers exhibited low accuracy for both HSI2 VIS and UAV VIS imagery (OA< 30.0%) while the overall accuracy for the HSI2 VIS+ NIR and Pleiades data ranged from 60.4%–78.4 % and 42.1%–66.4%, respectively, suggesting the importance of spectral range for the unsupervised classifiers.

ARTICLE HISTORY
Received 25 November 2017
Accepted 25 September 2018

CONTACT Prabha Amali Rupasinghe prabhar@bgsu.edu Department of Geology, Bowling Green State University, Bowling Green, OH, USA

1. Introduction

Mapping land and aquatic vegetation using remotely sensed imagery for better management and conservation of vegetation communities in coastal areas has been of long-standing interest in many parts of the world (Herdendorf 1987; Edsall and Charlton 1997). Due to natural complexity and heterogeneity of vegetation cover, various remote sensing sensors and techniques are utilized for monitoring coastal ecosystems over large areas at various time scales. Spatial and spectral properties of imagery acquired from spaceborne platforms commonly present a real challenge when mapping of mixed vegetation along a narrow strip of coastline is required (Milne 1988; Schmidt and Skidmore 2003; Shippert 2003; Xie, Sha, and Yu 2008; Adam and Mutanga 2009). For instance, Landsat is a widely used multispectral spaceborne sensor for mapping land cover (Bauer and Yuan 2004; Yuan et al. 2005; Souza et al. 2013); however, Landsat data are commonly inadequate for fine scale mapping of coastal vegetation due to its relatively coarse spatial resolution of 30 m (Xie, Sha, and Yu 2008; Ghioca-Robrecht, Johnston, and Tulbure 2008). The Satellite Pour l'Observation de la Terre (SPOT) multispectral imagery, with resolutions of 10 m and 20 m, provides better but still limited information (Rutchey and Vilchek 1999; Phillips, Beeri, and DeKeyser 2005). Only with the development of 'very high resolution' multispectral sensors, such as IKONOS (3.20 m resolution), QuickBird (2.40 m resolution), GeoEye (1.84 m resolution) or WorldView (0.31 m resolution), is the detailed mapping of coastal areas possible (Van der Sande, De Jong, and De Roo 2003; Wang et al. 2004).

The use of hyperspectral images for coastal monitoring overcomes the limitations of broad wavebands of multispectral imagery (Govender, Chetty, and Bulcock 2007). Their fine spectral resolution allows greater ability to differentiate more species and vegetation classes (Tsai and Philpot 2002; Govender et al. 2008; Ferrato and Forsythe 2013). While the spaceborne hyperspectral sensors (e.g. Hyperion and the decommissioned Project for On-Board Autonomy Compact High Resolution Imaging Spectrometer (PROBA CHRIS)) are better for large areas, the airborne hyperspectral sensors are more advantageous for ecosystem monitoring because of their finer spatial resolution (Anderson 1976). Due to the combination of high spatial and high spectral resolutions, several airborne hyperspectral sensors, such as Airborne Visible/Infrared Imaging Spectrometer (AVIRIS), Compact Airborne Spectrographic Imager (CASI), HyMap, and Airborne Hyperspectral Imaging System (AISA) are shown to be successful for coastal land cover mapping at the ecosystem level (Harsanyi and Chang 1994; Kokaly, Clark, and Livo 1998; Neuenschwander, Crawford, and Provancha 1998; Chan and Paelinckx 2008; Jones, Coops, and Sharma 2010). Several studies have used airborne hyperspectral data to map vegetation at the taxonomic level (Lawrence, Wood, and Sheley 2006), such as mapping of leafy spurge in the Theodore Roosevelt National Park (O'Neill et al. 2000), flowering leafy spurge in northeastern Wyoming (Williams and Hunt 2002), or hoary cress in Idaho (Mundt et al. 2005). Despite many advantages, a number of limitations are associated with hyperspectral data. These limitations include redundancy of information due to large number of correlated bands as well as long data-processing time and high computational cost, which requires a careful selection and implementation of processing algorithms to extract information (Landgrebe 2002; Simic and Chen 2008). Different processing and statistical techniques such as Vegetation Indices (VI) and Principal

Component Analysis (PCA) are commonly used to avoid these limitations (Subramanian et al. 1997; Landgrebe 2002; Rodarmel and Shan 2002; Govender, Chetty, and Bulcock 2007).

Constant development of classification algorithms requires their persistent evaluation. Both supervised and unsupervised classification methods are successfully used in various remote sensing applications. The advantage of using unsupervised classification methods is that a raw image is automatically converted into useful information (Tso and Olsen 2005), without time-consuming training data collection, a task difficult to accomplish in coastal wetlands with limited physical access (Ozesmi and Bauer 2002). Thus, many studies consider unsupervised classification methods for coastal areas (Shanmugam, Ahn, and Sanjeevi 2006; Butera 1983; Goodin 1995; Ill et al. 1998).

The supervised classification algorithms, on the other hand, require prior ground-based knowledge, which enhance the classification process and thus, they are commonly considered as advanced methods. The Maximum Likelihood Classification (MLC) algorithm was originally developed for classification of multispectral imagery but later it was also found to be applicable to hyperspectral imagery (Chang and Ren 2000; Butera 1983; Zainal, Dalby, and Robinson 1993; Yi et al. 1994). Kutching (2007) compared the MLC, neural network, decision tree, and spectral angle mapper classification methods for AISA images and obtained the best classification accuracy from MLC. While MLC has been successfully used in a wide range of land cover/land use mapping, the Support Vector Machines (SVM) method has attracted attention in recent years. Differently from MLC, which is a parametric method based on Bayesian approach, SVM is an optimization-based non-parametric machine learning method (Zhang, Ren, and Jiang 2015). Many studies showed the effectiveness of SVM for both hyperspectral and multispectral images (Gualtieri et al. 1999; Melgani and Bruzzone 2004; Pal and Mather 2005; Devadas, Denham, and Pringle 2012; Simic Milas et al. 2017). Due to a relatively competitive strength of the MLC and SVM methods, as shown in a number of previous studies, the performance of these two supervised classifiers appears to be different from one case study to another (Zhang, Ren, and Jiang 2015).

In the present study, two unsupervised (*k*-means and iterative self-organizing data analysis) and two supervised standard classifications, one based on parametric and another on non-parametric statistical approach (MLC and SVM, respectively) are applied to remote sensing imagery acquired by three different sensors: 1) recently developed second-generation airborne NASA Glenn Hyperspectral Imager (HSI2); 2) multispectral satellite sensors Pleiades; and 3) recently emerged Unmanned Aerial Vehicle (UAV) technology. The HSI2 sensor has been recently developed by NASA and its mapping capability is critical for several national studies conducted over coastal regions; however, there is no study on its performance and application for land cover classification. Thus, the first objective is to examine the performance of HSI2 to monitor land cover along the western coastal region of Lake Erie, USA. The HSI2 data were acquired in 2015 along the Western Lake Erie basin coastline as part of a collaborative effort between NASA and several universities in Ohio (Lekki et al. 2017). The second objective is to explore how different spectral ranges, and spatial and spectral resolutions of imagery collected over the coastal area impact the unsupervised and supervised classifiers. In particular, the classifications are applied to (*a*) the whole HSI2 hyperspectral dataset, which includes the visible and near-infrared (VIS+ NIR) bands, and to (*b*) the spectral subset that

includes only the visible (VIS) range. The overall accuracies are compared with the classification outcomes of Pleiades satellite multispectral data, which are collected over the VIS+ NIR spectral range, and with the UAV multispectral images acquired in the VIS range.

2. Methods

2.1. *Study area*

Lake Erie is one of the largest freshwater lakes in the world. It is ranked as ninth largest by surface area and fifteenth largest in world by volume (Herdendorf 1987). The lake is the shallowest of the Great Lakes and is 388 km long and 92 km wide with a mean depth of 19 m (Herdendorf 1992) (Figure 1). The shoreline is predominantly characterized by eroded banks of glacial till and lacustrine sediments with the rest of the area consisting of resistant bedrock bluffs (Herdendorf 1987). The mean annual air temperature for the Lake Erie region ranges from 8.4°C to 10.0°C. The highest temperatures, from 21.1°C to 23.4°C, are observed during July and the lowest temperatures, from −4.4°C to −2.2°C, are commonly observed in January and February. The average yearly rainfall ranges from 77 cm to more than 102 cm. The present study was conducted over twenty-two study sites along the western basin of Lake Erie, from Toledo, OH to Vermilion, OH. The study sites and the level of classification were chosen based on the requirements of a collaborative project between the University of Toledo, Bowling Green State University, and the Ohio Department of Natural Resources, which addressed the

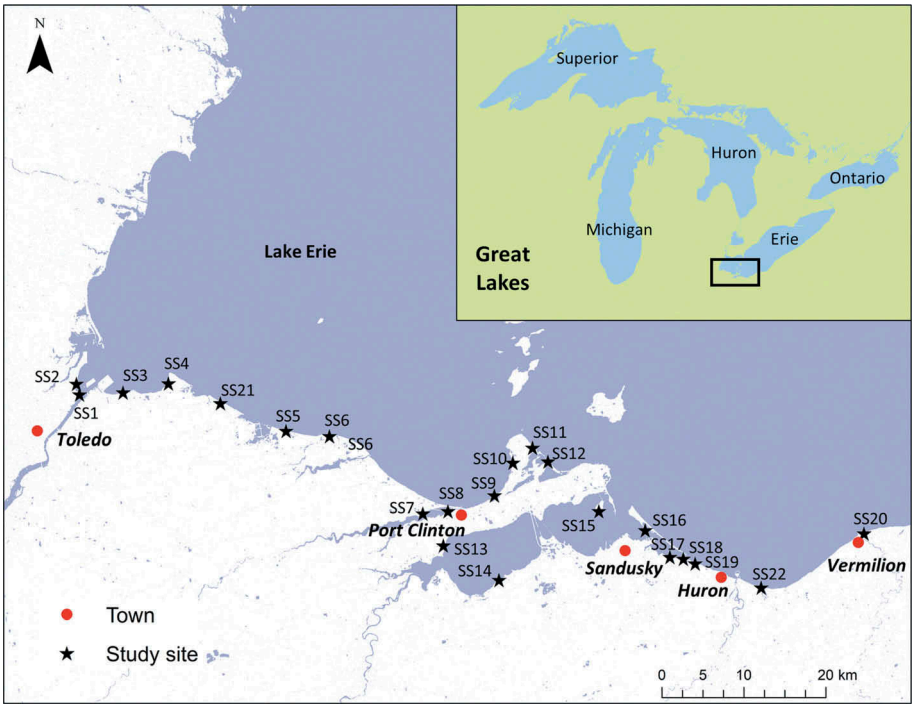

Figure 1. The Western Lake Erie basin with 22 study sites (SS) along the shoreline. (Source: U.S. Geological Survey, National Land Cover Database, 2011).

impact of the coastal land cover and vegetation types on fish abundance in Lake Erie (Figure 1, Table 1). Each study site included an area of about 500 m along the coastline and 50 m from the shoreline, inland and over the water.

2.2. *Remote sensing data*

2.2.1. *Field campaigns and ground truth data collection*

In collaboration with the University of Toledo, several field campaigns were completed concurrently with the NASA airborne campaigns from the end of July to early October 2015. To enhance atmospheric corrections of the HSI2 images, the field reflectance measurements of different land cover types such as terrestrial and aquatic vegetation, rocks, beach, tar roads, sandy roads, and concrete banks were collected using the handheld spectroradiometer PSR-3500 (Spectral Evolution 2017). The spectroradiometer covers the visible-near infrared-short infrared (VIS-NIR-SWIR) spectrum, with wavelengths ranging from 350 to 2500 nm, and spectral resolution of 3 nm from 350 nm to 700 nm, 8 nm from 700 nm to 1500 nm, and 6 nm from 1500 nm to 2500 nm. Given that we did not have major cost and time constraints, an extensive amount of ground data was collected during several field campaigns throughout the summer where sampling data were constantly improved and assembled into a comprehensive database containing more than 1000 sample points.

Table 1. The coordinates of study sites and land cover classes observed at each site. *Representative sites: Site 22 for UAV based classification; Sites 17, 18, and 19 for classification using HSI2 and Pleiades. Note: The selection is made based on the availability of data.

Site	Latitudes (°)	Longitudes (°)	Land cover classes
Site 1	41.6967	−83.4698	Buildings, grass, ground, lake, parking lots, tar roads, sand roads, aquatic vegetation, trees, shrubs
Site 2	41.7046	−83.4706	Aquatic vegetation, lake, buildings, grass, parking lots, tar roads, sand roads, trees
Site 3	41.6895	−83.4153	Concrete, grass, lake, parking lots, tar roads, rock, trees
Site 4	41.6913	−83.3463	Beach, wetlands, lake, rocks, sand roads, trees
Site 5	41.6264	−83.1778	Aquatic vegetation, beach, lake, rocks, sand roads, trees, wetland water
Site 6	41.6147	−83.1181	Beach, buildings, grass, lake, tar roads, shrubs, trees
Site 7	41.5161	−82.9933	Aquatic emergent vegetation, grass, ground, tar roads, lake, floating aquatic vegetation, shrubs, trees
Site 8	41.5154	−82.9606	Buildings, grass, lake, parking lots, rail road, bridge, rocks, sand roads, trees
Site 9	41.5307	−82.8736	Aquatic vegetation, buildings, concrete, grass, ground, lake, roads, shrubs, trees, lake
Site 10	41.5651	−82.8557	Beach, buildings, concrete, grass, lake, parking lots, tar roads, rocks, sand roads, trees
Site 11	41.5775	−82.8249	Beach, buildings, grass, lake, tar roads, rocks, shrubs, trees
Site 12	41.5502	−82.7970	Aquatic vegetation, concrete, grass, ground, lake, parking lots, tar roads, shrubs, trees, wetlands
Site 13	41.4792	−82.9682	Aquatic vegetation, ground, lake, rocks, trees, shrubs, trees, wetlands
Site 14	41.4241	−82.9132	Buildings, grass, ground, lake, tar roads, rocks, trees
Site 15	41.4890	−82.7406	Beach, boat ramps, buildings, grass, lake, tar roads, rocks, sand roads, tree
Site 16	41.4661	−82.6750	Beach, grass, lake, parking lots, tar roads, rocks, trees
Site 17*	41.4340	−82.6461	Aquatic vegetation, grass, lake, tar roads, sand roads, trees
Site 18*	41.4280	−82.6234	Aquatic vegetation, grass, lake, tar roads, rocks, trees
Site 19*	41.4225	−82.6104	Aquatic vegetation, beach, lake, rocks, shrub, trees, wetlands
Site 20	41.4274	−82.3524	Beach, buildings, grass, lake, parking lots, tar roads, rocks, sand roads, trees
Site 21	41.6296	−83.1892	Aquatic vegetation, beach, trees, grass, lake, rocks, sand roads, wetlands
Site 22*	41.6479	−83.2337	Aquatic vegetation, beach, buildings, creek, grass, ground, lake, tar roads, sand roads, trees

The sampling method used in the present study was based on the probability measure of classification accuracy (Foody 2002; Stehman 2009). The stratified random sampling approach based on geographic stratification by land cover class was used as the basic sampling design (Stehman 2009). For each site, *a priori* defined homogenous or near homogenous patches (polygons) and random sample locations (pixels), generated within each patch using Google Earth and HSI2 images via ArcGIS, were constantly refined in the field. New patches and sampling locations were being selected at each visit and added to the database. Vegetation phenology was also observed and used to enhance the sampling process. The Garmin GPS handheld field instrument (accuracy within 3 m) and Google Earth on mobile device were used to locate sample points in accessible areas and to approximate coordinates for inaccessible sites such as private lands, thickly forested regions and inaccessible swamps. Both planned, and opportunistically selected sample locations were based on a pixel as an assessment unit within each patch where each point was labelled as one class. At each site, the goal was to have two to three homogenous patches for each class, which size ranged from 5 × 5 m to 10 × 10 m, and to have minimum 3–4 sample locations within each patch. However, some small patches (e.g. 3 × 3 m) contained only one sampling point, in which case we increased a number of patches for a given class. To remind the reader, the level of classification and the number of classes were determined in advance based on the project's requirements. Table 1 shows the land cover classes observed at each study site. Although several sites had the same or similar land cover types, most of them were different. Originally, the goal was to keep the size and number of patches and sampling points similar across the land cover types; however, this was not always possible. Some land cover types covered small areas and had elongated patches and less sampling points (e.g. beaches along the shoreline, roads). Nevertheless, this did not present a major accuracy uncertainty due to insensitivity of the stratified sampling design to changes in sample size (Stehman 2009). The sample points were spatially well distributed being spread throughout the study sites without large gaps with the exception of the inaccessible areas.

By the end of summer, all points were mapped over the HSI2 and Google Earth images and the database was cleaned; duplicate and near-overlapping points were deleted. Data collected for each site and for each class were then interactively separated into training and validation subsets using the random sampling function in ArcGIS. We also explored several combinations of the random separations but did not observe any major impact on the accuracy assessments before selecting the final datasets. The training subsets contained from 29 to 32 sampling points while the validation subsets contained from 15 to 20 sampling points per site (135–180 pixels, considering the 3 × 3 windows). To reduce the bias caused by the sampling training and validation subsets from the same patches, the validation subset was enriched with additional pixels from selected 'validation only' patches. It should be noted that due to the limitation of the software (ENVI) processing capabilities to handle SVM, we had to reduce the number of samples per class to 15–20 for each site.

2.2.2. *Airborne hyperspectral NASA Glenn HSI2 images*

The NASA Glenn HSI2 sensor is a push broom, airborne, hyperspectral sensor with 170 spectral bands that cover the spectral range between 400 nm and 900 nm with the

spectral resolution of 2.5 nm (Table 2). The digitization bit depth is 14 bits. The field of view (FOV) of the sensor during the flights was 12.4° and the image rate was 25 frames per second. More information about the NASA Glenn HSI2 sensor is provided in the online NASA report (Lekki et al. 2017).

The sensor collected data with approximately a 1 m spatial resolution along the travel and perpendicular directions at 0.45 km altitude. The data were georeferenced to WGS 1984 UTM Zone 17N and were radiometrically calibrated by NASA (Lekki et al. 2017). In some cases, the sensor exhibited a near saturation response for high reflectance targets (e.g. sand, buildings, and water) for certain bands (Lekki et al. 2017), which were excluded from the analysis. The saturation was observed mostly in bands between ~700 to 800 nm or, in some rare cases, between ~550 to 650 nm. The NASA flight campaigns were organized bi-weekly or monthly. Images collected in July and August were used for the image classification. To convert the radiance values to reflectance, the images were atmospherically corrected using the empirical line calibration method in ENVI. The method was chosen based on our results, and it is in agreement with the recommended method by NASA (Lekki et al. 2017). As the reference site for atmospheric corrections of the HSI2 data, NASA selected the parking lot situated next to the Maumee Bay State Park (Figure 2). Field reflectance measurements of the white and dark background set by NASA were collected concurrently with the airborne data acquisitions and used as the light and dark targets, respectively, in the empirical line calibration. In some cases, the beach and dark still water at Site 4 were also considered (Figure 2).

Table 2. Specifications of NASA Glenn HSI2, Pleiades, and UAV sensors.

Sensors	HSI2	Pleiades	UAV
Data Type	Hyperspectral	Multispectral	Multispectral
Platform	Airborne	Spaceborne	Airborne
Spatial resolution	1 m	0.5 m panchromatic and 2 m multispectral	~0.32 m
Spectral bands	170 bands (400 to 900 nm)	Panchromatic (480–830 nm) and 4 bands (Blue: 430–550 nm, Green: 490–610 nm, Red: 600–720 nm, NIR: 750–950 nm)	3 bands (Blue: 400–500 nm, Green: 450–610 nm, Red (580–670 nm)
Altitude	0.45 km	694 km	0.12 km
Swath	258 m	20 km at nadir	300 m (overlap of 75%)

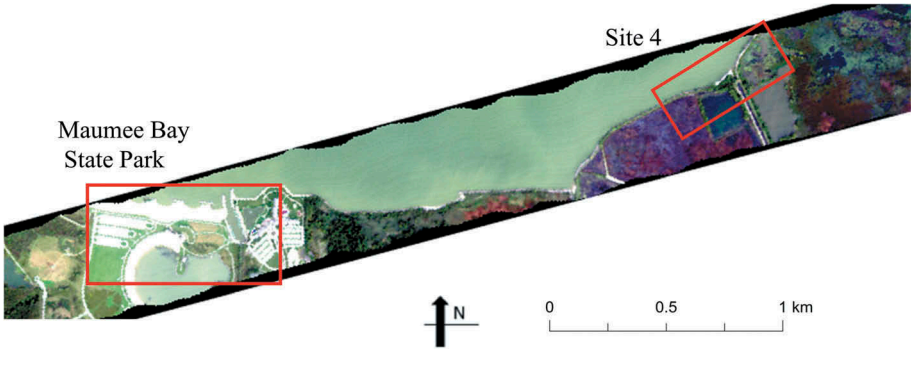

Figure 2. NASA Glenn HSI2 image acquired on 25 August 2015 over site 4 and the reference location near Maumee Bay State Park (1.6789° N, 83.3740° W). Note: Red squares indicate the areas under interest.

2.2.3. *Multispectral Pleiades and UAV images*

Pleiades, built by AIRBUS Defense and Space (Airbus 2015), consists of a constellation of twin satellites placed on the same orbit and phased 180° from each other. Each satellite has a multispectral system with a push broom scanner and daily revisit capability. Pleiades covers a 20-km swath with a standard viewing angle of ± 30°. Dynamic range at acquisition is 12 bits per pixel. The Pleiades product includes one panchromatic (spatial resolution is 0.50 m), and the multispectral bands (spatial resolution is 2 m) (Table 2). One Pleiades image was available for this study (Figure 3(a)). It was acquired on 20 May 2015 over three study sites: Sites 17, 18 and 19. Images were radiometrically corrected and ENVI FLAASH was used for atmospheric corrections to produce reflectance images (Harris Geospatial Docs Center 2017).

The eBee Ag Sensefly UAV with Canon RGB camera (SenseFly SA 2017) was used to collect data over Site 22 in September 2016 (Figure 3(b) and (c)). The eBee is a fixed-wing drone with a very lightweight of just 700 g (Table 2); it is easy to use as it allows for pre-launching flight preparation and simulations. The planning and control computer system eMotion was used to plan and fly the system (Drones For Professionals, Mapping & Photogrammetry, Flight Planning & Control Software: SenseFly SA 2017). The flight area ceiling was set up to 121.92 m, and the working radius was 2700 m. Lateral and longitudinal overlap was set to 75%. The flight lines spacing was 41.60 m, and the distance between acquired images was 30.70 m. Data were collected in a single flight. Fifty-one images were used in the processing. The images were mosaicked and orthorectified, and reflectance images were created for each RGB band using Pix4Dmapper Pro software (Pix4D 2018). The reflectance values were represented by DN values and were assumed to be equal to the radiance. In addition, the Visible Atmospherically Resistant Index (VARI) and Digital Surface Model (DSM) images were generated, which were fused in the process of classification (Stow, Niphadkar, and Kaiser 2005). More information about the processing of the UAV data can be found in the study of Simic Milas et al. (2017).

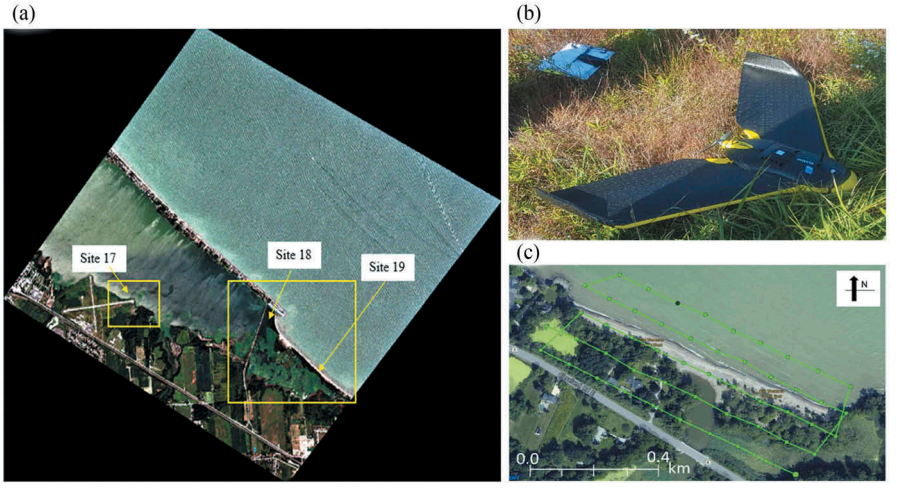

Figure 3. (a) Pleiades image acquired on 20 May 2015, including Sites 17, 18, and 19; (b) UAV eBee; (c) UAV collection points and flight lines (in green) over Site 22 (Old Woman Creek, Huron, Ohio); with permission from SimicMilas et al. (2017).

2.3. *Image classification*

Two unsupervised (*k*-means and Iterative Self-Organizing Data Analysis Technique (ISODATA)) and two supervised classifiers (MLC and SVM) were applied to (1) HSI2 imagery for twenty-two sites for two spectral ranges (*a*) VIS+ NIR that included all 170 bands (400–900 nm); (*b*) VIS that included 102 bands (400–700 nm); (2) one Pleiades image that contained three study sites (Sites 17 on one image and Sites 18 and 19 on another image), and (3) UAV data over one site (Site 22) (see Simic Milas et al. 2017) for more information on classification).

For both unsupervised classification methods, change threshold of 5% and 8 maximum number of iterations were used. For the ISODATA classification, the minimum number of pixels per class was set to 5 and the minimum number of merge pairs was set to 2. The number of classes for the unsupervised classifications were based on land cover types of each site. The post-classification labelling was done using information from field campaigns and Google Earth. In some cases, an additional class-merging process was performed for classes of very small size. This resulted in some minor differences in the number of classes between the different datasets. For MLC, no probability threshold was used, and data scale factor was set to 16,383. For the SVM classification, the radial basis function kernel with the parameter gamma was set to 0.01 and the penalty parameter was set to 200. Same number and the locations of training were used for both supervised classification methods for each site.

The number of land cover classes varied between 6 and 12 classes among the study sites. The common classes for most of the study sites included the lake, trees, grass, buildings, tar roads, and bare ground. Some sites had unique classes such as aquatic vegetation (Table 1). The effect of PCA on classification was additionally explored by applying the method to the HSI2 data prior to the classifications to reduce the information redundancy.

The classification validation was conducted using the validation sampling points and field sampling scheme as explained in Section 2.2.1. The same training and validation datasets were used for MLC and SVM. The overall classification accuracies (OA) of the HSI2 classified images were compared with the classification outcomes of multispectral Pleiades and UAV images. During the classification process, each Region-Of-Interest (ROI) (a.k.a. training site) located over the sampling location was set to 3 × 3 m to reduce the possible errors due to pixel locations (GPS coordinates) and mixed pixels. The basic objective of the accuracy assessments was to reach at least 80% overall accuracy. The accuracy assessment in this study was undertaken for the reason of providing an overall measure of the quality of the land cover map (Foody 2002).

3. Results

3.1. *Image classification of NASA Glenn HSI2 images*

The empirical line calibration method results in strong agreement between the field and image reflectance measurements for the HSI2 data with the correlation coefficient ranging from r = 0.86–0.92 for different land cover types and locations. Some minor discrepancies have been observed in the blue and NIR bands for different land cover classes such as sand and some types of vegetation (e.g. willow), when the images and

ground reflectance were compared, most likely due to the saturation effect that we and NASA observed in the original data.

Based on the OA and kappa coefficient values, the SVM classifier shows the best results for both datasets, when applied to the whole HSI2 dataset (VIS+ NIR) and for the spectral subset (VIS) (Table 3). SVM performs better than MLC for both datasets. Among the sites, the SVM related OA ranges between 82.6% and 97.5% with the average value of 85.58% for the HSI2 data VIS dataset. SVM exhibits insignificantly lower values for the VIS+ NIR dataset where OA ranges between 81.5% and 95.6% with the average value of 83.45% (Table 3). MLC related OA was somewhat lower ranging from 79.2% to 87.1% for VIS dataset and from 74.1% to 84.7% for VIS+ NIR dataset. Overall, the supervised classifiers used in the present study perform better than the unsupervised classifiers for both datasets with somewhat higher overall accuracy for VIS bands (Table 3). Moderate-to-strong OAs are observed for two unsupervised classification methods, ISODATA and *k*-means (OA = 69.9–78.4% with the average of 75.4 for ISODATA and 67.2–73.2% with the average of 69.2 for *k*-means, for the VIS+ NIR dataset across different sites) (Table 3). Neither of the two methods performs well for VIS bands (12.9%-20.3% with the average of 16.9% for ISODATA and 15.1%-28.5% with the average of 17.1 for *k*-means).

Table 4 provides the error matrix for SVM applied to HSI2 VIS dataset for Site 22 (Old Woman Creek, Huron, Ohio). The highest confusion is observed between trees and grass classes. Also, beach class is somewhat confused with tar roads and sand roads.

Figure 4 shows the user's and producer's accuracies for HSI2 data for different classifiers for Site 22. For the VIS dataset, SVM has the highest user and producer accuracies, closely followed by MLC. Both SVM and MLC for the VIS+ NIR dataset have on average slightly lower user's and producer's accuracies. Both ISODATA and K-mean classification for VIS data show very low user's and producer's accuracies for most of the classes while the accuracies greatly increased when VIS+ NIR data are used. The classified images for Site 22 are shown in Figure 5.

The SVM classification shows a slight improvement of up to 2.6% when PCA is used to decrease the number of input bands to 25. Rodarmel and Shan (2002) observed a similar improvement in their study when they applied PCA prior to classification of HYDICE and AVIRIS data.

3.2. *Classification of Pleiades and UAV images*

SVM also performs well for the Pleiades images (OA = 79.2–83.4% for three sites). However, the OA is lower than that obtained with the HSI2 VIS images (OA = 88.9–95.6% for the same

Table 3. Accuracy assessment of the HSI2 classified image for Site 22.

		VIS bands		VIS+ NIR bands	
Classification method		Overall accuracy (%)	Kappa coefficient	Overall accuracy (%)	Kappa coefficient
Unsupervised classification	ISODATA	18.4	0.3	78.3	0.7
	k-means	20.3	0.1	72.4	0.7
Supervised classification	SVM	88.0	0.8	85.3	0.8
	MLC	85.2	0.8	81.1	0.8

Table 4. Error matrix (by number of pixels) for HSI2 (VIS) dataset for the SVM classifier (Site 22).

	Lake	Trees	Grass	Creek	Tar roads	Sand roads	Beach	Buildings	Ground	Rocks	Aquatic grass	Floating aquatic	Total
Lake	**432**	0	0	17	0	0	3	0	0	0	0	0	452
Trees	0	**521**	48	14	0	1	0	0	0	0	1	9	594
Grass	0	19	**188**	0	0	0	0	0	2	0	0	3	212
Creek	12	0	0	**162**	0	0	0	0	0	0	2	2	178
Tar roads	0	1	0	0	**148**	4	0	16	0	12	0	0	181
Sand roads	0	0	0	0	0	**92**	17	5	0	0	0	0	114
Beach	0	0	0	0	21	10	**123**	0	18	0	1	3	176
Buildings	0	3	0	0	0	0	0	**249**	2	19	0	0	273
Ground	0	0	0	0	0	0	13	0	**351**	5	0	0	369
Rocks	2	0	0	0	0	2	0	8	0	**58**	0	0	70
Aquatic grass	0	6	8	2	0	0	0	0	0	0	**116**	11	143
Floating aquatic	0	2	12	4	0	0	0	0	0	0	8	**112**	138
Total	446	552	256	199	169	109	156	278	373	94	128	140	2900

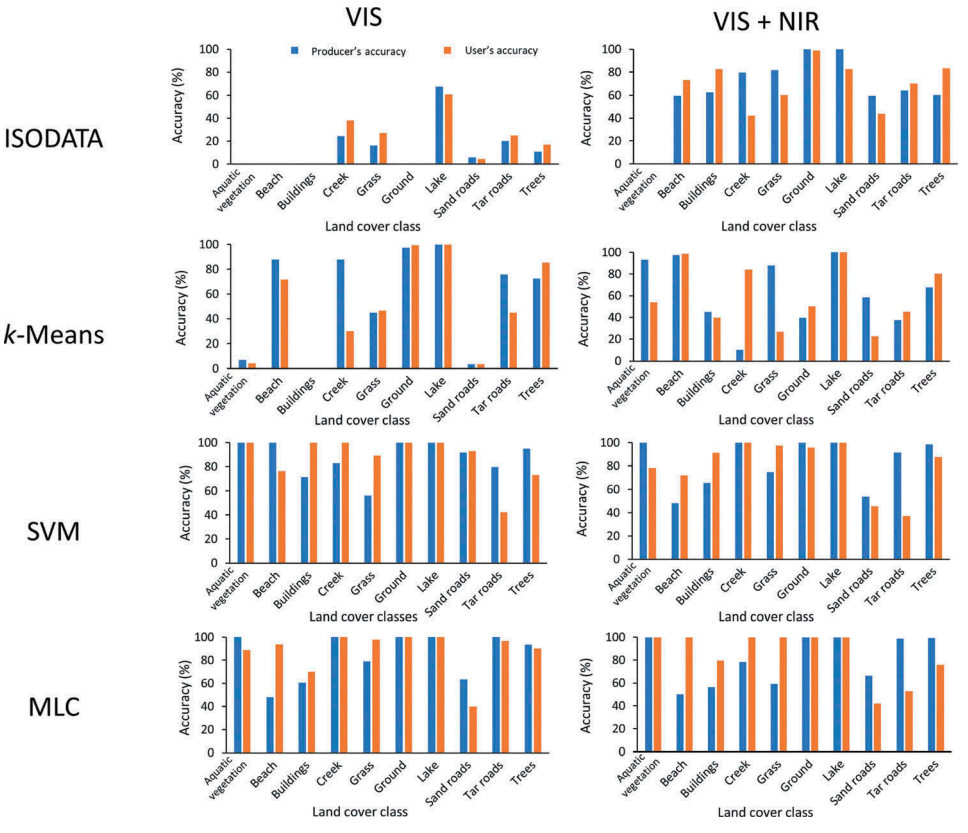

Figure 4. User's and producer's accuracy for the HSI2 images using supervised and unsupervised classifiers for site 22.

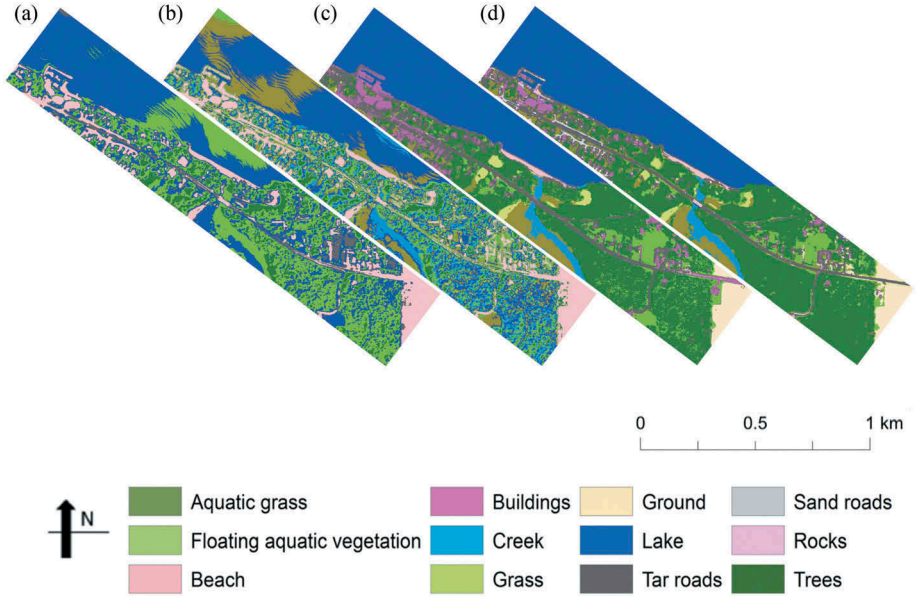

Figure 5. Classified NASA Glenn HSI2 images for site 22 (VIS) using several classifications: (a) *k*-means; (b) ISODATA; (c) MLC; (d) SVM.

three sites). The results are closely followed by MLC (Table 5). Overall, the supervised classification methods show notably higher accuracy for the HSI2 VIS images than for the Pleiades images. On the other hand, the unsupervised classifiers exhibit considerably higher OA for the Pleiades images (OA = 56.1–66.4% for *k*-means and OA = 42.1–52.4% for ISODATA classifier) (Table 5, Figure 6) suggesting the importance of the wider spectral range (VIS+ NIR) for the unsupervised classifiers. Although the same number of classes was originally used for the unsupervised and supervised classifications, several classes were either not detected or were merged in the last step of the unsupervised classification due to their small areal coverage creating a slight discrepancy in the results comparison.

Similarly, the same classes used for the HSI2 were considered for the UAV image except for rocks and sand roads, which were excluded due to a smaller area coverage of the UAV image. As described in the study by Simic Milas et al. (2017), unsupervised classification did not perform well for the UAV image in their study (OA = 28.8%). The authors found that SVM performed better than MLC for the UAV image (OA = 82.4% and OA = 79.3%, respectively) (Figure 7) (Simic Milas et al. 2017). The overall accuracy of SVM for the UAV data collected over Site 22 (OA = 82.4%) does not exceed the overall accuracy reached for the HSI2 image acquired over the same site (OA = 85.5%).

Table 5. Comparison of overall accuracy (OA) for NASA Glenn HSI2 VIS dataset (no NIR bands) and Pleiades imagery. Note: Sites 18 and 19 are located on the same image, next to each other and both sites are used simultaneously in the classification process.

	Overall accuracy and Kappa coefficients							
	HSI2 (Site 17)		Pleiades (Site 17)		HSI2 (Sites 18 and 19)		Pleiades (Sites 18 and 19)	
Classification method	Overall accuracy (%)	Kappa coefficient	Overall accuracy (%)	Kappa coefficient	Overall accuracy (%)	Kappa coefficient	Overall accuracy (%)	Kappa coefficient
ISODATA	20.1	0.1	52.4	0.4	18.3	0.1	42.1	0.3
k-means	27.3	0.2	66.4	0.6	21.2	0.1	56.1	0.5
MLC	82.8	0.7	79.5	0.7	85.4	0.8	74.8	0.8
SVM	**95.6**	**0.9**	**83.4**	**0.8**	**88.9**	**0.8**	**79.2**	**0.7**

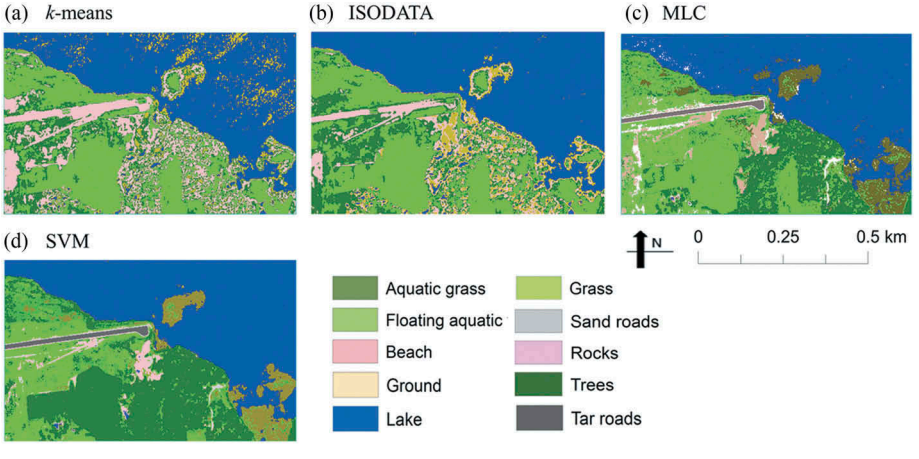

Figure 6. Classified Pleiades image using classifiers from Table 4 (Images are magnified for site 17).

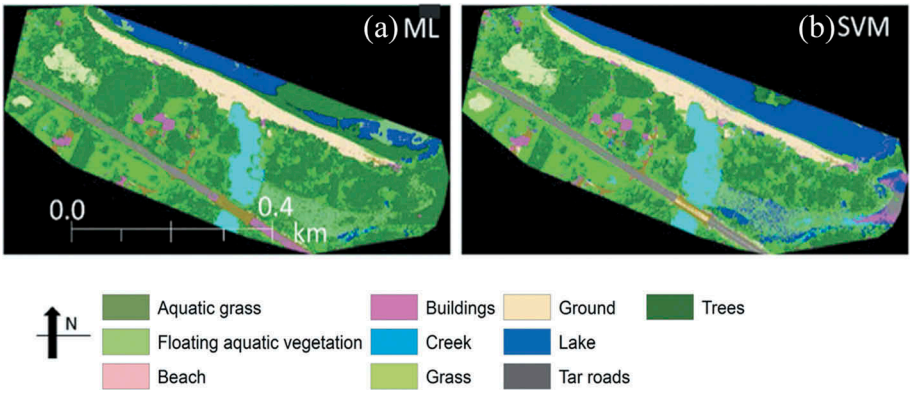

Figure 7. Classified UAV image for site 22 using (a) MLC; (b) SVM.
Source: With permission from SimicMilas et al. (2017).

4. Discussion

Remote sensing is a useful tool for land cover mapping along a coastline region; however, using a new sensor always represents a challenge for scientists. Development of classification algorithms using a new sensor requires a systematic performance evaluation. Classification of hyperspectral remotely sensed imagery, in particular, remains a challenge, due to many factors such as data redundancy and image processing and classification approaches (Lu and Weng 2007). While working with hyperspectral data, the user works with large datasets. Dimensionality reduction is commonly needed as it helps to minimize the redundant data and enhance the computation efficiency of classification (Rodarmel and Shan 2002).

The availability of the airborne hyperspectral, UAV and Pleiades images over the same area provided us with an opportunity to explore the effectiveness of several commonly used classifiers of different statistical nature on remote sensing data of different spectral range, and spectral and spatial resolutions. Although supervise classifications are often considered as more advanced methods, unsupervised classifiers should not be underestimated, as it may be less subjective, and they do not require training sites and foreknowledge of the classes, which may be particularly important for heterogenous, commonly non-accessible coastal areas.

The choice of the supervised classifiers in our study is based on several factors: 1) MLC and SVM classifiers have different underlying statistics, which is important to consider when exploring the performance of a new sensor such as HSI2 (Zhang, Ren, and Jiang 2015); 2) The two classifiers are commonly competing in their performance although SVM performed better for hyperspectral data in several studies (Chang and Ren 2000; Butera 1983; Zainal, Dalby, and Robinson 1993; Gi-Chul et al. 1994), and in many studies the MLC method serves as the baseline to which other classifiers are compared, as it yields high accuracy (Wulder and Franklin 2012); and 3) The sampling design and substantial field information have ensured the reliable performance of the MLC and SVM classifiers and accuracy assessments in this study. Although the number of samples was reduced during the SVM-based data processing due to the limitation of the software, SVM commonly demonstrates low variability for

different training datasets (Shao and Lunetta 2012), and high accuracy can be obtained by selecting a small training dataset collected in a proper way (Foody and Mathur 2004). SVM does not require the estimation of statistical distribution of land cover classes, and it is based on the margin examination between different land cover classes (Melgani and Bruzzone 2004).

The findings in this study are in accordance with several other studies (Pal and Mather 2005; Zhang, Ren, and Jiang 2015); the SVM method outperforms MLC for all three sensors regardless of the spectral range or spectral and spatial resolutions of the data. The same or similar trend is observed for all twenty-two sites. Eighteen sites exhibit 3% or higher OA values for SVM than for MLC. The best classification performance for both NASA Glenn HSI2 and Pleiades images is obtained with SVM and then with MLC, regardless of the presence of the NIR band in HSI2 imagery. Although the MLC method has been considered to perform better for the multispectral data, we observe comparatively higher classification accuracy for HSI2 than for Pleiades or UAV multispectral data. Yang et al. (2009) achieved overall accuracies of 94.7% when they applied MLC to AISA hyperspectral images to map black mangrove along the south Texas gulf coast. It should be noted that adding the NIR band in the HSI2 dataset, the classification accuracy insignificantly decreases. Although we cannot explain the trend, we surmise that the sensor borne uncertainty as mentioned above and explained in the NASA report (Lekki et al. 2017) may cause the trend (per communication with NASA).

The unsupervised classifications perform reasonably well when the NIR bands are included in the classification and very poorly when the NIR bands are excluded, suggesting that the spectral range of data (VIS+ NIR) is critical for unsupervised classifications. Although not very high, the accuracy of the unsupervised classifications for the Pleiades images (VIS + NIR) is reasonably higher than for the HSI2 VIS data, confirming better performance of unsupervised classifications over a larger spectral range as suggested in earlier studies (Butera 1983; Goodin 1995; Ill et al. 1998; Shanmugam, Ahn, and Sanjeevi 2006). As the spatial resolution of the HSI2 (1 m) is not considerably different from Pleiades (2 m), it can be suggested that the spectral resolution plays a more important role in image classification methods than the spatial resolution at a given scale. The importance of the NIR band should not be neglected in the classification of the Pleiades images to compensate for their wide spectral bands especially when we use unsupervised classification methods. The results suggest that the (hyper)spectral resolution of the HSI2 data for the subset (VIS) spectral range is favourable over the multispectral range (VIS+ NIR) of the Pleiades image and over spatial resolution of the UAV data (32 cm) for heterogeneous vegetated areas such as those seen in the Lake Erie coastal region.

The similarities of the OA values between the HSI2 VIS and UAV VIS classified images must be discussed in the context of shade effects. Although we expected to observe higher OA for the UAV data, the challenges due to shaded areas on the UAV image may be the reason for the results. As found by SimicMilas et al. (2017), the UAV image had a high coverage of shadows, and a special approach had to be applied to remove shadows in the process of classification. The FOV of the HSI2 data is 12.4°, and the Bidirectional Reflectance Distribution Function (BRDF) effect is not likely to be significant.

Although the findings related to HSI2 in this study are strong, the comparison of the results from the three sensors involves some uncertainties mostly due to different dates of image acquisitions. As above mentioned, the HSI2 and Pleiades images were collected

during the growing season and in May 2015, respectively, while the UAV image was acquired in September 2016. Changes in plant phenology between the seasons most likely affected the separability of the classes and the classification performance to a certain level. Also, we had only one site to compare the HSI2 and UAV classified images and three (other) sites to compare the HSI2 and Pleiades images. In addition, the UAV area is a subset of the area covered by HSI2. This decreases the certainty of our results; however, we believe that the pattern of our finding is consistent and having twenty-two sites covered with all three technologies would be a challenge to collect for any study.

As the basic objective of this study is overall and class-specific accuracy, the stratified sampling scheme is appropriate, and no major uncertainties are expected due to the sampling design (Stehman 2009). Some inconsistency of the sampling designed between land cover patches is not expected to introduce major uncertainties as explained earlier (Stehman 2009).

The errors introduced by pixel locations and mixed pixels commonly result in uncertainties; however, by applying 3×3 m large ROIs over the sampling pixels, it is expected that these errors are reduced. The errors caused by the atmospheric effects in the images are also minimal as we applied the most conservative (based on field reflectance measurements) atmospheric correction model for HSI2.

Despite all the errors, which are unavoidable in the classification processes, the fact that accuracy matrices behave similarly over all twenty-two sites, suggests that the error due to the sampling scheme, classifiers, georegistration and ground data accuracy are minimal and that the accuracy assessment can be trusted. Although one could assume that some uncertainties in the results could be associated with the different land cover types among the study sites, we believe that exactly the consistency of the results over the study sites strengthens the findings. This means that the classifiers used in the comparison are robust enough to capture the overall trend regardless of some differences in land cover types. After all, this has been the purpose of the study, to explore and propose a classification method that will be effective and suitable for the HSI2 data collected over the western Lake Erie basin. The study area is vast and applying one reliable classification method over the whole western shoreline of Lake Erie will be an advantage to other studies. The study has involved a commercial software and widely available classifiers for the reason of convenience and availability to other researchers.

SVM is a robust method that is successfully used for hyperspectral and multispectral data of high spatial resolution and over different spectral ranges (VIS or VIS+ NIR). SVM also exceeds our objectives of having OA $\geq$ 80%. The average OA value is $\geq$85%, the quality threshold commonly found in literature as summarized by (Foody 2008). We selected a somewhat lower OA threshold because the performance of the sensor was not widely known, and some uncertainties in data processing (as explained above) were observed. The accuracy interpretation for most of the classes does not differ considerably, which adds a positive note to the accuracy assessment (Foody 2008). The trade-off between the spectral and spatial resolutions and spectral range is observed mostly between the HSI2 VIS data and the Pleiades multispectral data (VIS+ NIR) where the spectral resolution rather than spectral range is a prevailing factor for better overall accuracy. A very fine spatial resolution of the UAV (VIS) data is not shown as advantageous over the HSI2 VIS data in our study. The recently emerged UAV technology, however, requires more research to show that the classification algorithms are

transferable from satellite and airborne hyperspectral data to the fine spatial resolution of a couple of cm. Georeferencing and proper mosaicking of the UAV images require additional improvements within this technology to be able to propose an optimal spatial resolution for a given classification algorithm.

Overall, our study shows that the machine learning SVM method outperforms unsupervised and MLC classifications for all three sensors. It performs slightly better than MLC and considerably better than ISODATA and *k*-means unsupervised classifiers. Although based on two different statistical approaches, both supervised classifiers, MLC and SVM, perform better for all three datasets when compared to the unsupervised classifiers, especially for the hyperspectral data. We surmise that high heterogeneity of the study area has a negative effect on the unsupervised classifiers in this study.

5. Conclusion

This study evaluated the performance of the standard unsupervised (*k*-means and ISODATA) and supervised (MLC and SVM) classification algorithms applied to the NASA Glenn HSI2 images and compared the results with Pleiades and UAV data. The SVM classification was identified as the best classification algorithm for HSI2, Pleiades and UAV data. The classifiers used in the comparison are robust enough to capture the overall trend regardless of the sensor types and differences in land cover types among twenty-two study sites included in the HSI2 related analysis. To examine the trade-offs between the spectral and spatial resolution as well as spectral range, two HSI2 datasets (spatial resolution of 1.00 m) were considered: (1) one with all available spectral bands (VIS+ NIR), and (2) one with a spectral subset (VIS). Classifications based on both datasets were included in the classification processes and then compared with the results generated using the multispectral Pleiades (VIS + NIR) and UAV (VIS) with a spatial resolution of 2.00 m and 0.32 m, respectively. Significantly better classification accuracy of SVM for the hyperspectral data collected in the VIS spectral range over the Pleiades multispectral data collected in the VIS and NIR region suggested that better results were achieved with hyperspectral data but limited to the VIS spectral range than with multiple bands collected over the VIS and NIR spectral region. Similar results were obtained with MLC. The unsupervised classifiers, on the other hand, were found to be more appropriate for the full spectral range (VIS+ NIR). The unsupervised algorithms exhibited low accuracy for both HSI2 VIS and UAV VIS datasets regardless of the differences in their spectral and spatial resolutions. Overall, the hyperspectral resolution of the HSI2 images acquired over the VIS spectral region was shown to be advantageous over (1) the larger spectral range of the Pleiades images (VIS+ NIR) and (2) the higher spatial resolution of UAV image acquired in the (VIS) spectral region for which shaded areas may introduce unexpected uncertainties.

Acknowledgments

This project was funded by the National Oceanic and Atmospheric Administration (NOAA), Ohio Division of Natural Resources (ODNR) and University of Toledo. Authors also gratefully acknowledge National Aeronautics and Space Administration (NASA) for providing data. We thank Roger P. Tokars,

Robert C. Anderson, John D. Lekki, Mr. Larry C. Liou (NASA Glenn Research Center) and Ms. Terri Benko for establishing the collaboration.

Disclosure statement

No potential conflict of interest was reported by the authors.

Funding

This work was supported by the National Oceanic and Atmospheric Administration U.S Department of Commerce through the Ohio Coastal Management Program, administered by the Department of Natural Resources, Office of Coastal Management [NA13NOS4190057]; Ohio Division of Natural Resources; University of Toledo.

References

Adam, E., and O. Mutanga. 2009. "Spectral Discrimination of Papyrus Vegetation (Cyperus Papyrus L.) In Swamp Wetlands Using Field Spectrometry." *ISPRS Journal of Photogrammetry and Remote Sensing* 64 (6): 612–620. doi:10.1016/j.isprsjprs.2009.04.004.

Anderson, J. R. 1976. "A Land Use and Land Cover Classification System for Use with Remote Sensor Data. Vol. 964." US Government Printing Office. Accessed March 15. https://books.google.ca/books?hl=en&id=dE-ToP4UpSIC&oi=fnd&pg=PA1&dq=Anderson,+J.+R.+(1976).+A+land+use+and+land+cover+classification+system+for+use+with+remote+sensor+data+(Vol.+964).+US+Government+Printing+Office.&ots=sWqq_X1f4E&sig=bcC7c7fbzdrUvkhSyztASJVzf6Q.

Bauer, M. E., and F. Yuan. 2004. "Cities (Minnesota) Metropolitan Area." In Proceedings of the Second International Workshop on the Analysis of Multi-Temporal Remote Sensing Images: Multitemp 2003, Joint Research Centre, Ispra, Italy, 16-18 July 2003, 3, 368.World Scientific. https://books.google.ca/books?hl=en&id=as5gDQAAQBAJ&oi=fnd&pg=PA368&dq=Bauer,+M.+E.,+Yuan,+F.,+%26Sawaya,+K.+E.+(2003,+July).+Multi-temporal+Landsat+image+classification+and+change+analysis+of+land+cover+in+the+Twin+Cities+(Minnesota)+metropolitan+area.+In+Proceedings,+MultiTemp-2003,+Second+International+Workshop+on+the+Analys&ots=mG8doLQe-s&sig=_MwUd8YYQIeR2IPSaTf3cPT1UOY.

Butera, M. K. 1983. "Remote Sensing of Wetlands." *IEEE Transactions on Geoscience and Remote Sensing*, no. 3: 383–392. doi:10.1109/TGRS.1983.350471

Chan, J. C.-W., and D. Paelinckx. 2008. "Evaluation of Random Forest and Adaboost Tree-Based Ensemble Classification and Spectral Band Selection for Ecotope Mapping Using Airborne Hyperspectral Imagery." *Remote Sensing of Environment* 112 (6): 2999–3011. doi:10.1016/j.rse.2008.02.011.

Chang, C.-I., and H. Ren. 2000. "An Experiment-Based Quantitative and Comparative Analysis of Target Detection and Image Classification Algorithms for Hyperspectral Imagery." *IEEE Transactions on Geoscience and Remote Sensing* 38 (2): 1044–1063. doi:10.1109/36.841984.

Devadas, R., R. J. Denham, and M. Pringle. 2012. "Support Vector Machine Classification of Object-Based Data for Crop Mapping, Using Multi-Temporal Landsat Imagery." *The International Archives of the Photogrammetry, Remote Sensing and Spatial Information Sciences* 39: 185–190. doi:10.5194/isprsarchives-XXXIX-B7-185-2012.

Edsall, T. A., and M. N. Charlton. 1997. "Nearshore Waters of the Great Lakes." Environment Canada. Accessed March 15. https://archive.epa.gov/solec/web/pdf/nearshore_waters_of_the_great_lakes.pdf.

Ferrato, L.-J., and K. W. Forsythe. 2013. "Comparing Hyperspectral and Multispectral Imagery for Land Classification of the Lower Don River, Toronto." *Journal of Geography and Geology* 5 (1): 92. doi:10.5539/jgg.v5n1p92.

Foody, G. M. 2002. "Status of Land Cover Classification Accuracy Assessment." *Remote Sensing of Environment* 80 (1): 185–201. doi:10.1016/S0034-4257(01)00295-4.

Foody, G. M. 2008. "Harshness in Image Classification Accuracy Assessment." *International Journal of Remote Sensing* 29 (11): 3137–3158. doi:10.1080/01431160701442120.

Foody, G. M., and A. Mathur. 2004. "Toward Intelligent Training of Supervised Image Classifications: Directing Training Data Acquisition for SVM Classification." *Remote Sensing of Environment* 93 (1–2): 107–117. doi:10.1016/j.rse.2004.06.017.

Ghioca-Robrecht, D. M., C. A. Johnston, and M. G. Tulbure. 2008. "Assessing the Use of Multiseason QuickBird Imagery for Mapping Invasive Species in a Lake Erie Coastal Marsh." *Wetlands* 28 (4): 1028–1039. doi:10.1672/08-34.1.

Gi-Chul, Y., D. Risley, M. Koneff, and C. Davis. 1994. "Development of Ohio's GIS-Based Wetlands Inventory." *Journal of Soil and Water Conservation* 49 (1): 23–28.

Goodin, D. G. 1995. "Mapping the Surface Radiation Budget and Net Radiation in a Sand Hills Wetland Using a Combined Modeling/Remote Sensing Method and Landsat Thematic Mapper Imagery." *Geocarto International* 10 (2): 19–29. doi:10.1080/10106049509354488.

Govender, M., K. Chetty, and H. Bulcock. 2007. "A Review of Hyperspectral Remote Sensing and Its Application in Vegetation and Water Resource Studies." *Water Sa* 33 (2): 145–151.

Govender, M., K. Chetty, V. Naiken, and H. Bulcock. 2008. "A Comparison of Satellite Hyperspectral and Multispectral Remote Sensing Imagery for Improved Classification and Mapping of Vegetation." *Water SA* 34 (2): 147–154.

Gualtieri, J. A., S. R. Chettri, R. F. Cromp, and L. F. Johnson. 1999. "Support Vector Machine Classifiers as Applied to AVIRIS Data." Proceedings of Eighth JPL Airborne Geoscience Workshop. https://pdfs.semanticscholar.org/83e3/788925a7a78bcc89a4540c8808f8e2b7acb0.pdf.

Harris Geospatial Docs Center. 2017. "Atmospheric Correction (Using ENVI) [Harris Geospatial Docs Center]." Accessed Mar 14. http://www.harrisgeospatial.com/docs/AtmosphericCorrection.html#Log.

Harsanyi, J. C., and C.-I. Chang. 1994. "Hyperspectral Image Classification and Dimensionality Reduction: An Orthogonal Subspace Projection Approach." *IEEE Transactions on Geoscience and Remote Sensing* 32 (4): 779–785. doi:10.1109/36.298007.

Herdendorf, C. E. 1987. *The Ecology of the Coastal Marshes of Western Lake Erie: A Community Profile*. DTIC Document. Accessed 20 October 2017. http://oai.dtic.mil/oai/oai?verb=getRecord&metadataPrefix=html&identifier=ADA323024.

Herdendorf, C. E. 1992. "Lake Erie Coastal Wetlands: An Overview." *Journal of Great Lakes Research* 18 (4): 533–551. doi:10.1016/S0380-1330(92)71321-5.

Ill, E., W. Ramsey, D. K. Chappell, D. M. Jacobs, S. K. Sapkota, and D. G. Baldwin. 1998. "Resource Management of Forested Wetlands: Hurricane Impact and Recovery Mapped by Combining Landsat TM and NOAA AVHRR Data." *Photogrammetric Engineering & Remote Sensing* 64 (7): 733–738.

Jones, T. G., N. C. Coops, and T. Sharma. 2010. "Assessing the Utility of Airborne Hyperspectral and LiDAR Data for Species Distribution Mapping in the Coastal Pacific Northwest, Canada." *Remote Sensing of Environment* 114 (12): 2841–2852. doi:10.1016/j.rse.2010.07.002.

Kokaly, R. F., R. N. Clark, and K. E. Livo. 1998. "Mapping the Biology and Mineralogy of Yellowstone National Park Using Imaging Spectroscopy." In Summaries of the 7th Annual JPL Airborne Earth Science Workshop, 1, 21–97. Pasadena, CA: JPL Publication. https://aviris.jpl.nasa.gov/proceedings/workshops/98_docs/29.pdf.

Kutching, S. 2007. "The Performance of Maximum Likelihood, Spectral Angle Mapper, Neural Network and Decision Tree Classifiers in Hyperspectral Image Analysis." *Journal of Computer Science* 3 (6): 419–423. doi:10.3844/jcssp.2007.419.423.

Landgrebe, D. 2002. "Hyperspectral Image Data Analysis." *IEEE Signal Processing Magazine* 19 (1): 17–28. doi:10.1109/79.974718.

Lawrence, R. L., S. D. Wood, and R. L. Sheley. 2006. "Mapping Invasive Plants Using Hyperspectral Imagery and Breiman Cutler Classifications (Randomforest)." *Remote Sensing of Environment* 100 (3): 356–362. doi:10.1016/j.rse.2005.10.014.

Lekki, J., R. Anderson, D. Avouris, J. Churnside, M. Cline, J. Demers, J. Leshkevich, et al. 2017. "Airborne Hyperspectral Sensing of Armful Algal Blooms in Great Lakes Region: System Calibrationand Validation." Technical Report NASA/TM-2017-219071, E-19202, GRC-E-DAA-TN29647. Cleveland, OH: NASA Glenn Research Center. Accessed 1st November 2017. ntrs.nasa.gov/search.jsp?R=20170002298.

Lu, D., and Q. Weng. 2007. "A Survey of Image Classification Methods and Techniques for Improving Classification Performance." *International Journal of Remote Sensing* 28 (5): 823–870. doi:10.1080/01431160600746456.

Melgani, F., and L. Bruzzone. 2004. "Classification of Hyperspectral Remote Sensing Images with Support Vector Machines." *IEEE Transactions on Geoscience and Remote Sensing* 42 (8): 1778–1790. doi:10.1109/TGRS.2004.831865.

Milne, A. K. 1988. "Change Direction Analysis Using Landsat Imagery: A Review of Methodology." In *International Geoscience and Remote Sensing Symposium, Remote Sensing: Moving Toward the 21st Century,* Edinburgh, UK, 1, 541–544. doi:10.1109/IGARSS.1988.570193.

Mundt, J. T., N. F. Glenn, K. T. Weber, T. S. Prather, L. W. Lass, and J. Pettingill. 2005. "Discrimination of Hoary Cress and Determination of Its Detection Limits via Hyperspectral Image Processing and Accuracy Assessment Techniques." *Remote Sensing of Environment* 96 (3): 509–517. doi:10.1016/j.rse.2005.04.004.

Neuenschwander, A. L., M. M. Crawford, and M. J. Provancha. 1998. "Mapping of Coastal Wetlands via Hyperspectral AVIRIS Data." In *Geoscience and Remote Sensing Symposium Proceedings, 1998. IGARSS'98. 1998 IEEE International*, Piscataway, NJ, 1, 189–191. IEEE. http://ieeexplore.ieee.org/abstract/document/702848/.

O'Neill, M., S. L. Ustin, S. Hager, and R. Root. 2000. "Mapping the Distribution of Leafy Spurge at Theodore Roosevelt National Park Using AVIRIS." In *Proceedings of the Ninth JPL Airborne Earth Science Workshop*, 00–18. Pasadena, California, NASA Jet Propulsion Laboratory. http://aviris.jpl.nasa.gov/proceedings/workshops/00_docs/ONeill_web.pdf.

Ozesmi, S. L., and M. E. Bauer. 2002. "Satellite Remote Sensing of Wetlands." *Wetlands Ecology and Management* 10 (5): 381–402. doi:10.1023/A:1020908432489.

Pal, M., and P. M. Mather. 2005. "Support Vector Machines for Classification in Remote Sensing." *International Journal of Remote Sensing* 26 (5): 1007–1011. doi:10.1080/01431160512331314083.

Phillips, R. L., O. Beeri, and E. S. DeKeyser. 2005. "Remote Wetland Assessment for Missouri Coteau Prairie Glacial Basins." *Wetlands* 25 (2): 335–349. doi:10.1672/10.

Pix4D 2018. "Generate 2D and 3D Information, Purely from Images with Pix4D." *Pix4D*. Accessed June 13. https://pix4d.com/.

Rodarmel, C., and J. Shan. 2002. "Principal Component Analysis for Hyperspectral Image Classification." *Surveying and Land Information Science* 62 (2): 115.

Rutchey, K., and L. Vilchek. 1999. "Air Photointerpretation and Satellite Imagery Analysis Techniques for Mapping Cattail Coverage in a Northern Everglades Impoundment." *Photogrammetric Engineering and Remote Sensing* 65 (2): 185–191.

Schmidt, K. S., and A. K. Skidmore. 2003. "Spectral Discrimination of Vegetation Types in a Coastal Wetland." *Remote Sensing of Environment* 85 (1): 92–108. doi:10.1016/S0034-4257(02)00196-7.

SenseFly SA. 2017. "Drones for Professionals, Mapping & Photogrammetry, Flight Planning & Control Software: SenseFly SA." Accessed March 14. https://www.sensefly.com/home.html.

Shanmugam, P., Y.-H. Ahn, and S. Sanjeevi. 2006. "A Comparison of the Classification of Wetland Characteristics by Linear Spectral Mixture Modelling and Traditional Hard Classifiers on Multispectral Remotely Sensed Imagery in Southern India." *Ecological Modelling* 194 (4): 379–394. doi:10.1016/j.ecolmodel.2005.10.033.

Shao, Y., and R. S. Lunetta. 2012. "Comparison of Support Vector Machine, Neural Network, and CART Algorithms for the Land-Cover Classification Using Limited Training Data Points." *ISPRS Journal of Photogrammetry and Remote Sensing* 70: 78–87. doi:10.1016/j.isprsjprs.2012.04.001.

Shippert, P. 2003. "Introduction to Hyperspectral Image Analysis." *Online Journal of Space Communication* 3. Accessed 1 November 2017. https://spacejournal.ohio.edu/pdf/shippert.pdf.

Simic, A., and J. M. Chen. 2008. "Refining a Hyperspectral and Multiangle Measurement Concept for Vegetation Structure Assessment." *Canadian Journal of Remote Sensing* 34 (3): 174–191.

SimicMilas, A., K. Arend, C. Mayer, M. A. Simonson, and M. Scudder. 2017. "Different Colours of Shadows: Classification of UAV Images." *International Journal of Remote Sensing* 38 (8–10): 3084–3100. doi.org/10.1080/01431161.2016.1274449

Souza, C. M. Jr., J. V. Siqueira, M. H. Sales, A. V. Fonseca, J. G. Ribeiro, I. Numata, M. A. Cochrane, C. P. Barber, D. A. Roberts, and J. Barlow. 2013. "Ten-Year Landsat Classification of Deforestation and Forest Degradation in the Brazilian Amazon." *Remote Sensing* 5 (11): 5493–5513. doi:10.3390/rs5115493.

Spectral Evolution. 2017. "Spectral Evolution, Inc. — Field Spectrometer and Spectroradiometer Products for Remote Sensing." Accessed Mar 14. http://www.spectralevolution.com/portable_spectroradiometer.html.

Stehman, S. V. 2009. "Sampling Designs for Accuracy Assessment of Land Cover." *International Journal of Remote Sensing* 30 (20): 5243–5272. doi:10.1080/01431160903131000.

Stow, D., M. Niphadkar, and J. Kaiser. 2005. "MODIS-Derived Visible Atmospherically Resistant Index for Monitoring Chaparral Moisture Content." *International Journal of Remote Sensing* 26 (17): 3867–3873. doi:10.1080/01431160500185342.

Subramanian, S., N. Gat, M. Sheffield, J. Barhen, and N. Toomarian. 1997. "Methodology for Hyperspectral Image Classification Using Novel Neural Network." *AeroSense'97*, 128–137. International Society for Optics and Photonics. Accessed 2 November 2017. http://proceedings.spiedigitallibrary.org/proceeding.aspx?articleid=926204.

Tsai, F., and W. D. Philpot. 2002. "A Derivative-Aided Hyperspectral Image Analysis System for Land-Cover Classification." *IEEE Transactions on Geoscience and Remote Sensing* 40 (2): 416–425. doi:10.1109/36.992805.

Tso, B. R. A. N. D. T., and R. I. C. H. A. R. D. C. Olsen. 2005. "Combining Spectral and Spatial Information into Hidden Markov Models for Unsupervised Image Classification." *International Journal of Remote Sensing* 26 (10): 2113–2133. doi:10.1080/01431160512331337844.

Van der Sande, C. J., S. M. De Jong, and A. P. J. De Roo. 2003. "A Segmentation and Classification Approach of IKONOS-2 Imagery for Land Cover Mapping to Assist Flood Risk and Flood Damage Assessment." *International Journal of Applied Earth Observation and Geoinformation* 4 (3): 217–229. doi:10.1016/S0303-2434(03)00003-5.

Wang, L., W. P. Sousa, P. Gong, and G. S. Biging. 2004. "Comparison of IKONOS and QuickBird Images for Mapping Mangrove Species on the Caribbean Coast of Panama." *Remote Sensing of Environment* 91 (3): 432–440. doi:10.1016/j.rse.2004.04.005.

Williams, A. P., and E. R. Hunt. 2002. "Estimation of Leafy Spurge Cover from Hyperspectral Imagery Using Mixture Tuned Matched Filtering." *Remote Sensing of Environment* 82 (2): 446–456. doi:10.1016/S0034-4257(02)00061-5.

Wulder, M. A., and S. E. Franklin. 2012. *Remote Sensing of Forest Environments: Concepts and Case Studies*. Springer Science & Business Media. Boston, MA: Kluwer Academic publishers.

Xie, Y., Z. Sha, and M. Yu. 2008. "Remote Sensing Imagery in Vegetation Mapping: A Review." *Journal of Plant Ecology* 1 (1): 9–23. doi:10.1093/jpe/rtm005.

Yang, C., J. H. Everitt, R. S. Fletcher, R. R. Jensen, and P. W. Mausel. 2009. "Evaluating AISA+ Hyperspectral Imagery for Mapping Black Mangrove along the South Texas Gulf Coast." *Photogrammetric Engineering & Remote Sensing* 75 (4): 425–435. doi:10.14358/PERS.75.4.425.

Yuan, F., K. E. Sawaya, B. C. Loeffelholz, and M. E. Bauer. 2005. "Land Cover Classification and Change Analysis of the Twin Cities (Minnesota) Metropolitan Area by Multitemporal Landsat Remote Sensing." *Remote Sensing of Environment* 98 (2): 317–328. doi:10.1016/j.rse.2005.08.006.

Zainal, A. J. M., D. H. Dalby, and I. S. Robinson. 1993. "Monitoring Marine Ecological Changes on the East Coast of Bahrain with Landsat TM." *Photogrammetric Engineering and Remote Sensing; (United States)* 59 (3). http://www.osti.gov/scitech/biblio/6444251.

Zhang, Y., J. Ren, and J. Jiang. 2015. "Combining MLC and SVM Classifiers for Learning Based Decision Making: Analysis and Evaluations." *Computational Intelligence and Neuroscience* 2015. doi:10.1155/2015/423581.